Surfaces and Interfaces 21 (2020) 100674

Contents lists available at ScienceDirect

Surfaces and Interfaces

journal homepage: www.elsevier.com/locate/surfin

# Molecular dynamics simulations of separator-cathode interfacial thermal transport in a Li-ion cell

Abhijeet Dhakane[a], Vikas Varshney[b], Juan Liu[c], Hendrik Heinz[c], Ankur Jain[a,*]

[a] Mechanical and Aerospace Engineering Department, University of Texas at Arlington, 500 W First St, Rm 211, Arlington, TX 76019, USA
[b] Materials and Manufacturing Directorate, Air Force Research Laboratory, Wright-Patterson Air Force Base, OH, USA
[c] Department of Chemical and Biological Engineering, University of Colorado, Boulder, CO 80309, USA

ARTICLE INFO

*Keywords:*
Molecular dynamics Simulations
Interfacial thermal transport
Li-ion cell
Molecular bridging

ABSTRACT

While Li-ion cells show outstanding electrochemical performance, their poor thermal transport characteristics result in reduced performance as well as significant safety concerns. The heterogeneous interface between cathode and separator plays a vital role in the process of thermal conduction in a Li-ion cell. Recent experiments have shown that the cathode-separator interfacial thermal resistance contributes significantly to total thermal resistance within the cell. In this paper, thermal conductance across the cathode-separator interface is calculated using molecular dynamics (MD) simulations with IFF-CVFF force field. Thermal transport in a pristine heterogeneous interface as well as when bridged with 3-Aminopropyl triethoxysilane (APTES), n-Butyl trimethoxysilane (nBTMS) and 3-Mercaptopropyl trimethoxysilane (MPTMS) molecules is computed. It is shown that molecular bridging at the interface results in up to 250% improvement in interfacial thermal conductance for the APTES case, which is consistent with recent experimental data. These results quantify the key role of the cathode-separator interface in thermal transport within the Li-ion cell, as well as the potential improvement in interfacial thermal transport by molecular bridging. The techniques and results discussed here may help downselect molecular species for interfacial thermal transport enhancement in Li-ion cells.

## 1. Introduction

Li-ion cells are used widely in a large number of energy storage applications, including electric vehicles, consumer electronics, renewable energy storage, etc. [1,2]. High energy storage density is a key advantage of Li-ion cells compared to other energy storage technologies. Energy storage in a Li-ion cell occurs via intercalation and de-intercalation of Li ions between a cathode material, typically made of a Li salt such as $LiCoO_2$, $LiFePO_4$, etc. and an anode, typically made of graphite [2]. The anode and cathode are typically separated by a polymer-based separator. A roll or multiple folds of cathode-separator-anode-separator sheets are packed tightly into cylindrical or prismatic cells. A large number of such cells are electrically connected with each other to make a module and battery pack capable of large-scale energy storage [3].

Poor thermal transport in Li-ion cells and battery packs has been widely recognized to be a key technological concern that limits the use of Li-ion cells [4,5]. Overheating in Li-ion cells, often caused by poor thermal conductance within the cell, results in large temperature rise in the cell. Above a certain threshold, high cell temperature causes an increased rate of heat generation due to exothermic decomposition processes, which in turn raises the cell temperature further. This positive feedback phenomena, called thermal runaway, is unsustainable and results in catastrophic failure and fire [6,7].

It is clearly desirable to better understand and enhance thermal transport within a Li-ion cell for improved safety and performance. While a number of thermal management strategies have been investigated for external thermal management of Li-ion cells [4,8,9,10], thermal transport within the cell is known to be a rate-limiting step [7,11,12,13] and therefore, must be fully understood and optimized. In addition to being orthotropic, overall thermal conductivity of Li-ion cells has been measured to be very poor, of the order of 0.2-0.6 $Wm^{-1}K^{-1}$ [14,15]. Past work has demonstrated multiple benefits of improving thermal conductivity of the cell, including reduced likelihood of thermal runaway [12], increased discharge rate capability [11], increased energy storage density through reduced requirement for external thermal management [16], etc.

Given that most constituent materials within a Li-ion cell have reasonably high thermal conductivity [13,17], the overall poor thermal conductivity indicates dominance of interfacial thermal resistance [13].

* Corresponding author.
*E-mail address:* jaina@uta.edu (A. Jain).

https://doi.org/10.1016/j.surfin.2020.100674
Received 17 March 2020; Received in revised form 18 August 2020; Accepted 2 September 2020
Available online 08 September 2020

**Nomenclature**

| | |
|---|---|
| $m$ | molar mass (g/mol) |
| $v$ | velocity (Å/fs) |
| $k_b$ | Boltzmann Constant ($kgm^2/s^2K$) |
| T | Temperature (K) |
| λ | Interfacial Thermal Conductance ($MW/m^2$-K) |
| $\dot{Q}$ | Heat flux ($W/m^2$) |

Recently reported experimental measurements show that interfacial thermal resistance at the cathode-separator interface constitutes about 88% of overall thermal resistance within a Li-ion cell [13]. Using acoustic mismatch theory [18], such high resistance has been explained on the basis of presence of only weak van der Waals interactions at the interface and high mismatch in speeds of sound in the two materials [13]. However, a detailed explanation using more fundamental thermal transport simulations is missing. Further, measurements have shown that interfacial thermal transport between the cathode and separator can potentially be improved through molecular bridging between the two materials [13]. Interfacial bridging with aminosilane has been shown to result in 3X reduction in measured thermal contact resistance [13]. This is consistent with other experiments that report similar thermal enhancement with the use of molecular bridging between other material pairs such as Cu and $SiO_2$ [19], and Au and carbon nanotubes [20].

Given the length-scales (~few nm) associated with thermal transport at the molecular interfaces, molecular dynamics (MD) simulations are routinely used to investigate such transport and gain deeper understanding of heat conduction across the interfaces. For example, MD simulations have been employed to model thermal transport across a variety of material pairs such as graphene-semiconductor heterostructures [21], Si/Ge interfaces [22], silicene/silica interfaces [23], graphene/phosphorene interfaces [24], etc. A number of MD studies have also suggested that interfacial thermal transport can be enhanced by incorporating bridging molecules [19,25,26]. However, the literature specific to MD-simulations for thermal transport in Li-ion cell materials is rather sparse [27,28], particularly for interfacial thermal transport, mainly due to the lack of appropriate force-fields for cathode and other electrochemical materials. It is not clear which bridging molecules are most suitable for the specific materials that constitute the cathode and separator in a Li-ion cell. Given the large number of potential molecules that could be used as molecular bridges, it is important to develop computation tools to characterize thermal performance of various molecules towards enhanced interfacial thermal transport in a Li-ion cell. Such a tool will help down-select candidate molecules, which can then be characterized experimentally. Such a capability is particularly important in the context of Li-ion cells because of the time-consuming nature of experiments needed to establish long-term reliability and safety of any material changes within the cell.

This paper presents a MD based study of interfacial thermal resistance between $LiCoO_2$ cathode and amorphous polyethylene separator of a Li-ion cell. Specifically, the impact of incorporating three different molecules from the silane family at the cathode-separator interface on interfacial thermal resistance is presented. It is found that there may be substantial improvement in thermal transport at the cathode-separator interface by the use of a carefully selected bridging molecule due to end group interaction with the organic site. Results from this work are consistent with past experimental measurements [13], and may help select and design appropriate materials for improved thermal performance of Li-ion cells.

## 2. Simulation details

### 2.1. Material system

$LiCoO_2$ and amorphous polyethylene are investigated in this work because these are the most common constituents for cathode and separator, respectively for a Li-ion cell. In addition to a baseline case, where $LiCoO_2$ and polyethylene are directly attached to each other, a number of cases with presence of a bridging molecule are investigated.

Fig. 1(a)-(c) present the three alkylsilane molecules - APTES (3-Aminopropyl) triethoxysilane, MPTMS (3-mercaptopropyl) triethoxysilane and nBTMS (n-butyl) trimethoxysilane – investigated in this study for the interfacial thermal transport enhancement. The primary reason for choosing alkylsilanes for this study is the observation that they are known to self-assemble on metal oxide surfaces. This characteristic of alkylsilanes has been used in the past to adjust surface morphology, leading to altered wetting and transport properties [29-32]. Past experimental work also indicates the possibility of reduced interfacial thermal resistance due to similar molecules in a variety of material systems [13,19,20,33,34], most likely due to enhanced surface adhesion caused by functional sites on both ends of the molecule. Here, a molecular dynamics study of interfacial thermal transport in the presence of three such molecules is carried out. Comparative calculations of interfacial thermal transport without and with such molecules helps understand the relative thermal performance of such molecules.

### 2.2. Development of $LiCoO_2$ force field

While parameters for several organic molecules are well-established in literature, the parameters for $LiCoO_2$ are developed in this work using the following general outline for the Interface Force-Field (IFF) [35, 36] in CVFF format [37,38]: First, a small supercell structure for $LiCoO_2$ is created using available X-ray data from literature. Atom types, atomic charges, 'initial' bonded parameters, and Lenard-Jones parameters for all atoms are then assigned. Hereby, atomic charges accurately describe the chemistry and chemical bonding in the mixed oxide [39]. MD simulations are then carried out in order to analyze density and lattice constants of modeled structure. If the standard error is greater than 1% compared to experimental data, parameters are adjusted and the process is repeated. Otherwise, surface properties such as surface energy and solvation energy are computed, with a standard error of up to 5% considered acceptable. Mechanical properties are then

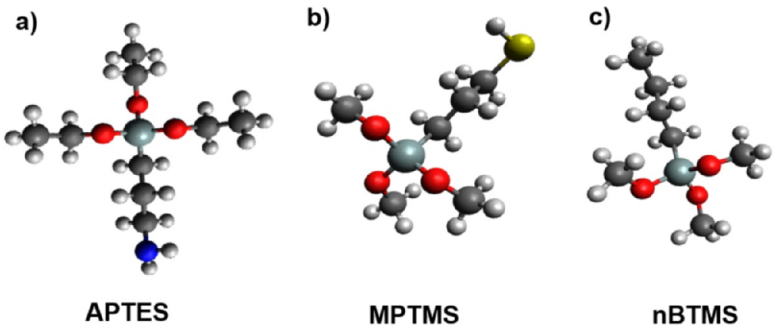


**Fig. 1.** Molecular structures of bridging molecules investigated in this work for functionalization of the cathode-separator interface. a) APTES [3-Aminopropyl triethoxysilane] b) MPTMS [3-Mercaptopropyl trimethoxysilane] c) nBTMS [n-Butyl trimethoxysilane]. (Colour scheme: Si-Cyan, C- Gray, H-White, O-Red, N-Blue, S-Yellow)

computed to further refine parameters, and usually obtained in good agreement with experiment without further major modifications. Developed parameters for $LiCoO_2$ for this study represent chemical bonding with experimental lattice geometry (error < 1%), density (error < 1%), mechanical properties (error < 5%) and cleavage energy (consistent with DFT calculation). The unit cell of $LiCoO_2$ models used in this work and the validations of CVFF are shown in Fig. 2. The structural properties were calculated from a 50 ps simulation in the NPT ensemble under 1.013 MPa and 298.15 K. The average lattice parameters and density are in good agreement with the experimental value with < 1% error [40]. Mechanical properties (bulk modulus and shear modulus) were further calculated in using the Forcite module in Material Studio[46]. The DFT calculated bulk modulus values were in a range from 143 (local density approximation, LDA) to 169 GPa (generalized gradient approximation, GGA) [41]. The reported experimental value is 149 GPa which was measured by high-pressure synchrotron XRD [41]. The average computed bulk modulus with CVFF is 161 GPa (< 5% error). Comparing with the experimental shear modulus 80 GPa obtained from pulse-echo measurement [42], the calculated value of 84 GPa also shows excellent match. Furthermore, surface properties are validated by the cleavage energy. The computed cleavage energy is determined by the difference in total energy between cleaved surface and bulk surface with the use of Discover in Material Studio in a NVT ensemble at 298.15 K. While there is no available experimental value of cleavage energy to compare, the computed cleavage energy of 0.95 J/m$^2$ is within the range of the reference data (0.93-1.03 J/m$^2$) from DFT calculations. The IFF force field parameters for $LiCoO_2$ (in CVFF format) thus obtained are summarized in Table 1 [35]. In principle, the IFF protocol for $LiCoO_2$ can be adopted to other functional forms (such as CHARMM and PCFF), and the complete IFF battery material force field for multiple energy expressions and chemistries will be described in a separate future publication. CVFF is chosen here due to its simplicity, leading to lower computational costs for simulation, as well as the observation that this force-field is well-studied for organic molecules and polymeric systems [43, 44]. In these simulations, the interaction between different organics and $LiCoO_2$ is considered physical in nature via van der Waals interaction. Interactions between different atom types are calculated as per CVFF force-field convention, enabled by the thermodynamic consistency of IFF parameters.

**Table 1**
$LiCoO_2$ IFF parameters in CVFF format.

| I. Non-bond | Atomic charge (e) | $\sigma$ (pm) | $\varepsilon$ (kcal•mol$^{-1}$) |
|---|---|---|---|
| Li | +0.62 | 173 | 0.04 |
| O | -0.80 | 345 | 0.15 |
| Co | +0.98 | 450 | 0.04 |
| II. Bond | $r_{o,\ ij}$ (pm) | | $K_r$ (kcal•mol$^{-1}$•Å$^{-2}$) |
| Co-O | 239 | | 118 |
| III. Angles | $\theta_{o,\ ijk}$ (°) | | $K_\theta$ (kcal•mol$^{-1}$•rad$^{-2}$) |
| ∠Co-O-Co | 98 | | 85 |
| ∠O1-Co-O1 | 98 | | 85 |
| ∠O2-Co-O2 | 98 | | 85 |
| ∠O1-Co-O2 | 84.5 | | 0 |

### 2.2. Simulation process

LAMMPS [45] package is used for all simulations. In addition to $LiCoO_2$, CVFF is used to model amorphous polyethylene and functionalization molecules. In order to create the structure of $LiCoO_2$-polyethylene system, an orthogonal cell of size (~ 28 × 28 × 72 Å) is created in Materials Studio for $LiCoO_2$ [46]. The amorphous polyethylene separator is modeled with 40 (-$CH_2$-) monomers of 47 chains built in MS 7.0 using amorphous polymer builder of similar size. Partial charge calculations for amorphous polyethylene and functionalize molecules are performed using Discover program in Material Studio . The PPPM (particle-particle-particle-mesh) model with energy tolerance of $1 \times 10^{-5}$ is used to incorporate long-range electrostatic interactions [47]. A distance cutoff of 12.0 Å is used for all simulations. The initial $LiCoO_2$-polyethylene system is relaxed by using NVT ensemble with 1.0 fs time step for integration for 1 ns. The final coordinates are used for the interfacial properties study.

$LiCoO_2$ and amorphous polyethylene structures are brought close enough to form an interface. The periodicity in lateral directions (*x*- and *y*- direction) mimic bulk-like interface conditions. The resultant structure is minimized with conjugate gradient algorithm, followed by heating at 300 K using NVT ensemble via Nose-Hoover thermostat as implemented in LAMMPS. An NPT (isothermal − isobaric) ensemble (Nose-Hoover thermostat/barostat) is then used to equilibrate the pressure and density with independent barostats along the orthogonal *x, y*, and *z* directions. The system is determined to be equilibrated until average energy is not changing with time and the energy fluctuations are minimized. All simulations are performed with 1fs time step.

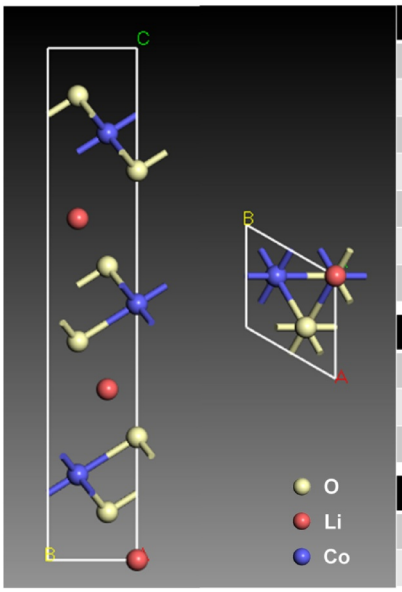


| Lattice geometry | | |
|---|---|---|
| | Expr. | IFF-CVFF (error) |
| a (Å) | 2.816 | 2.802 (0.5%) |
| b (Å) | 2.816 | 2.802 (0.5%) |
| c (Å) | 14.054 | 14.050 (0.1%) |
| α=β (°) | 90 | 90 (0) |
| γ (°) | 120 | 120 (0) |
| Density (g/cm$^3$) | 5.056 | 5.1 (0.9%) |

| Mechanical properties | | |
|---|---|---|
| | Expr. / DFT | IFF-CVFF (error) |
| Bulk modulus (GPa) | 149±2 / 143-169 | 161±2 (4.5%) |
| Shear modulus (GPa) | 80±1 | 84±2 (5%) |

| Surface properties | | |
|---|---|---|
| | Expr. / DFT | IFF-CVFF (error) |
| Cleavage energy (J/m$^2$) | NA / 0.93-1.03 | 0.95 (3%) |

**Fig. 2.** Model of a $LiCoO_2$ unit cell and the validation of developed parameters in IFF. The IFF-CVFF parameters were refined to reproduce the structural, energetic (cleavage energy), and mechanical properties.

Interfacial thermal conductance calculations across the $LiCoO_2$ and amorphous polyethylene with and without molecular bridging are performed using non-equilibrium molecular dynamics (NEMD) simulations on an orthogonal structure based on Fourier's law of heat conduction [48]. Fig. 3 shows a representative image of the molecular assembly for the baseline case of thermal transport through the cathode-separator interface without a bridging molecule. In contrast with this baseline case, Fig. 4(a) shows a representative image of the molecular assembly with molecular bridging across the cathode-separator interface, while Fig. 4(b) shows representative images of equilibrated bridging molecules near the interface for 10, 20 and 30 molecule case for APTES. Within the orthogonal slab constructed for simulation, the end edges of size 0.7 nm are fixed and excluded from all calculations, which leads to a quasi-2D periodic system. Further, 1 nm bins on the left and right ends are set to be hot and cold reservoir maintained at 350 K and 250 K, respectively, using temperature rescaling algorithm resulting in one dimensional heat flow.

In theory, the temperature gradient across the model system should be kept as minimal as possible to reduce the non-linearity in heat transport. However, in MD simulations, especially for interface thermal simulations, such a gradient is necessary due to few reasons: a) the error in instantaneous temperature within a bin is proportional to $\frac{1}{\sqrt{N}}$, ($N$ is number of atoms in the bin), which, for generic NEMD bin sizes is of the order of ~5-10K. In this case, the larger temperature difference would increase signal (temperature gradient) to noise (error in temperature) ratio; b) for interface thermal conductance simulations, it is necessary to have noticeable temperature difference at the interface between two heterogeneous media for accurate prediction. For systems that are not very conductive (such as epoxy) or having large interface resistance, this will entail large temperature difference at the boundaries; and c) while, in principle one could reduce the temperature at the boundaries significantly, such reduction will also reduce the cumulative heat flux, which will increase the error in calculation of heat flux (due to larger instantaneous fluctuations reducing signal to noise ratio). It should be noted that such order of temperature difference (~100 K) has often been reported previously in context of interface thermal conductance simulations [34,49].

As heat flows from left to right, energy is continuously added to and removed from the hot and cold reservoirs respectively to maintain their respective temperatures. Micro-canonical (NVE) ensemble is used in the non-fixed region of the simulation space in order to conserve the energy of the total system and eventually establish a steady state thermal gradient between the two reservoirs. The simulation space is divided into a number of 2 Å segments along the heat flux direction. Temperature of each segment is estimated by equating the total kinetic energy of each segment with average energy based on the Boltzmann number as follows:

$$\frac{1}{2}\Sigma m_i v_i^2 = \frac{3}{2}k_b T_i \tag{1}$$

where $m_i$, $v_i$ and $T_i$ are the mass, velocity and temperature of the atoms in the $i^{th}$ segment, respectively, and, $k_b$ is the Boltzmann constant.

A linear temperature distribution is expected in each material in the simulation space once steady-state is established. In addition, an abrupt temperature drop $\Delta T$ is expected at the interface due to heterogeneity of the molecular system. Here, the interfacial thermal conductance can be calculated using

$$\lambda = \frac{Q/\Delta t}{A\Delta T} \tag{2}$$

where $\lambda$, $Q/\Delta t$, and $A$ are thermal conductance, heat flow per unit time at the interface, and lateral cross-sectional area, respectively. $Q/\Delta t$ is calculated by taking the average absolute slope of cumulative energy added and subtracted to maintain the hot and cold reservoir temperatures. Each simulation is carried out for 5 ns to achieve steady state, at which point, the temperature distribution is determined in order to calculate heat flux, and the interfacial thermal conductance.

## 3. Results and discussion

We start our discussion with results from NEMD simulations for the baseline configuration with no bridging molecules (please refer to Fig. 3 for schematic representation). In this regard, Fig. 5 plots the partial cumulative energy profile added to and subtracted from the cold and hot thermostats, respectively, over the simulation period for baseline configuration. Once thermal fluctuations in the system are minimized and average slopes of both cumulative energies reach similar values, indicating steady-state. Temperature distribution in the system is calculated as described in Section 2, and is plotted in Fig. 6.

As expected, Fig. 6 shows lower temperature gradient on the cathode side than separator side, due to the relatively higher thermal conductivity of $LiCoO_2$. Past measurements have shown that cathode thermal conductivity is expected to be around 3-5 $Wm^{-1}K^{-1}$ [33], compared to 0.5 $Wm^{-1}K^{-1}$ for the separator [50]. Fig. 5 also shows a significant temperature drop at the interface, which is associated with thermal resistance at the interface between cathode and the separator. Based on the observed temperature drop (17.7 K), heat flow (2.61 $kcalmol^{-1}ps^{-1}$) and lateral surface area (823.51 $Å^2$), the interfacial thermal conductance is estimated to be 125 ± 13 $MWm^{-2}K^{-1}$ (interface thermal resistance of 0.008 $m^2K(MW)^{-1}$). In the rest of the paper, these results are taken as the baseline for comparison with cases where alkylsilane bridging molecules are present across the interface. The reported values are in agreement (similar order of magnitude) with other MD studies reported for thermal transport across heterogeneous interfaces [19,21-24,39,44]. It should be noted that MD reported values of interfacial thermal conductance are often notably higher than experimental measurements, partly due to the ideal conditions of interfaces being modeled in MD simulations (flat interfaces, no pits, etc.) In addition, it should also be noted that while the absolute values of predicted quantities depend significantly on force-fields used, often, observed trends in such quantities provide key insights about the responsible molecular phenomena, such as how different molecular interactions, molecular topology (orientation, alignment, etc.), crystallinity or amorphousness of the two media, surface roughness, etc. affect

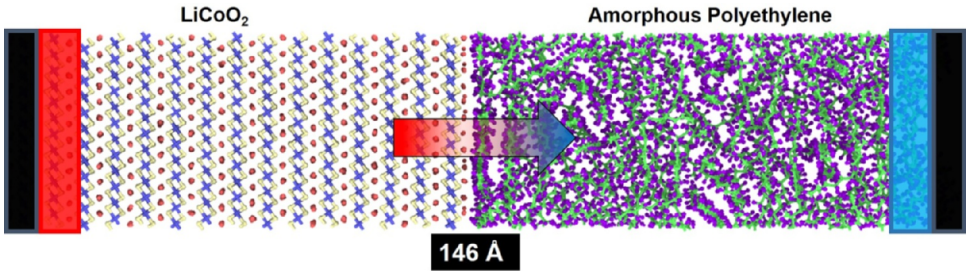


**Fig. 3.** Molecular structure for simulation of the baseline case for $LiCoO_2$-polyethylene interface without a bridging molecular layer. Hot reservoir (red rectangle on left) and cold reservoir (blue rectangle on right) maintained at 350K and 250K respectively are shown.

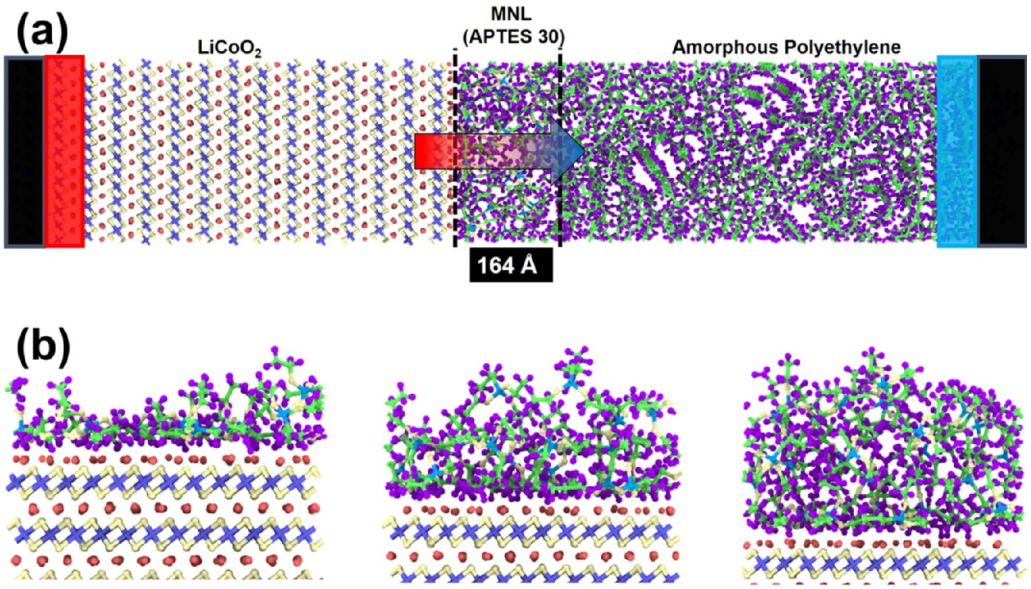


**Fig. 4.** (a) Molecular structure for simulation of a case with a bridging molecular layer (30 APTES molecules) at the $LiCoO_2$-polyethylene interface. Hot reservoir (red rectangle on left) and cold reservoir (blue rectangle on right) maintained at 350K and 250K respectively are shown. (b) Schematics of the cathode-APTES interface for simulations with 10, 20 and 30 molecules. Interface with amorphous polyethylene has been excluded for better clarity.

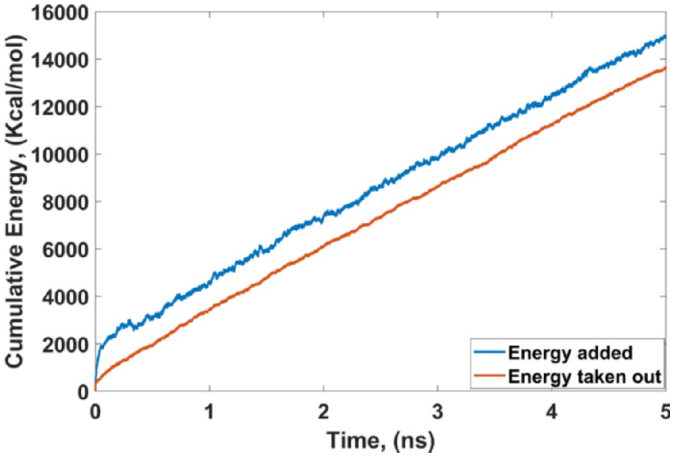


**Fig. 5.** Absolute cumulative energies added to and removed from hot and cold thermostats, respectively, as a function of simulation time.

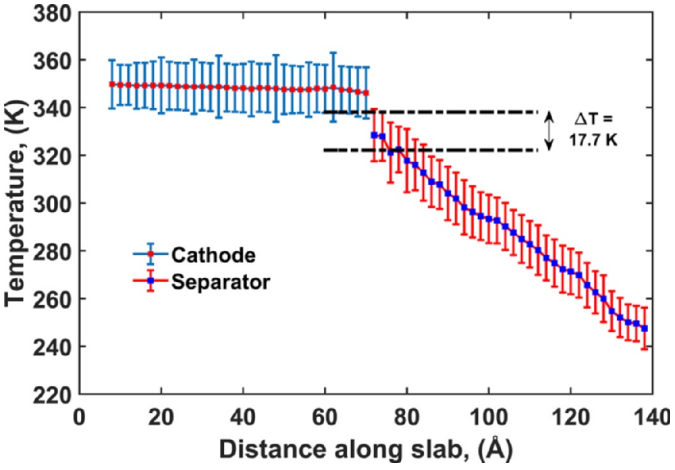


**Fig. 6.** Computed temperature distribution in the cathode and separator for the baseline case across the modeled slab.

interfacial thermal transport.

Next, simulations are carried out to investigate the impact of presence of three different alkylsilane molecules –APTES, MPTMS and nBTMS– between the cathode and separator (please refer to Fig. 4 for schematic representation). The number of molecules available at the interface is varied in order to evaluate the effect of incorporating different thicknesses of the molecules on interfacial thermal resistance. The silane functional site on one end of each of these molecules is expected to exhibit affinity towards metal oxides such as $LiCoO_2$, resulting in strong bonding on the cathode side. The functional group on the other end of these molecules is an amine group [$-NH_3$] for APTES, thiol [-SH] group for MPTMS and methyl [$-CH_3$] group for nBTMS, which likely interact with the amorphous polyethylene with varying degrees of affinity.

Surface functionalization with APTES molecules has been shown in past experiments [13] to result in 3X improvement in interfacial thermal resistance between cathode and separator. In order to investigate this through simulations, cases with 10, 20 and 30 APTES molecules between the cathode and separator are computed first. Simulation results are summarized in Fig. 7. Fig. 7 shows that while the baseline interfacial thermal conductance is around 125 $MW/m^2K$, there is significant improvement when the interface is bridged by APTES molecules. With 10, 20 and 30 molecules, the improvement in interfacial thermal conductance is around 176%, 84% and 250%, respectively. Fig. 7 also shows error estimates of the computed thermal contact conductance. The large error estimate for 10 and 30 APTES molecule cases is primarily attributed to lower temperature difference (higher interface thermal conductance) and noisier temperature (in relation to other cases) profile near at the interface.

The general improvement in interfacial thermal conductance due to the presence of APTES molecules is consistent with past experiments on the same material system [13], and may be explained on the basis of APTES end group affinities towards $LiCoO_2$ and amorphous polyethylene. While amine groups are well attracted towards the organic polyethylene, the silane group on the other end of APTES may facilitate stronger bonding with $LiCoO_2$ compared to the baseline case with only weak van der Waals bonding. It should also be noted that we do not see a monotonically increasing trend in interface thermal conductance, as expected. The possible origin of such non-monotonicity is summarized later in this paper after discussing interface thermal conductance results of all molecules.

Similar simulations are carried out for MPTMS molecule, which has a thiol group at one end instead of silane, as shown in Fig. 1(b). Simulation results are shown in Fig. 8. Compared to the APTES molecule,

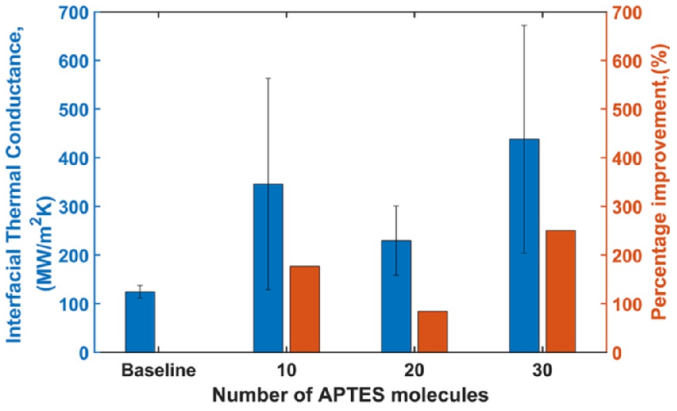


**Fig. 7.** Comparison of computed interfacial thermal conductance for 10, 20 and 30 APTES molecules with the baseline case without molecular bridging.

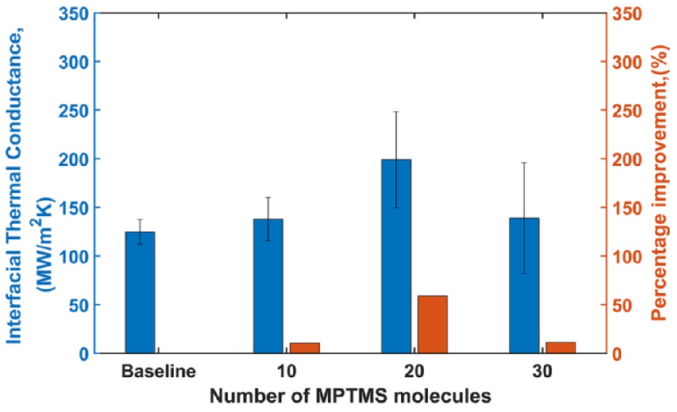


**Fig. 8.** Comparison of computed interfacial thermal conductance for 10, 20 and 30 MPTMS molecules with the baseline case without molecular bridging.

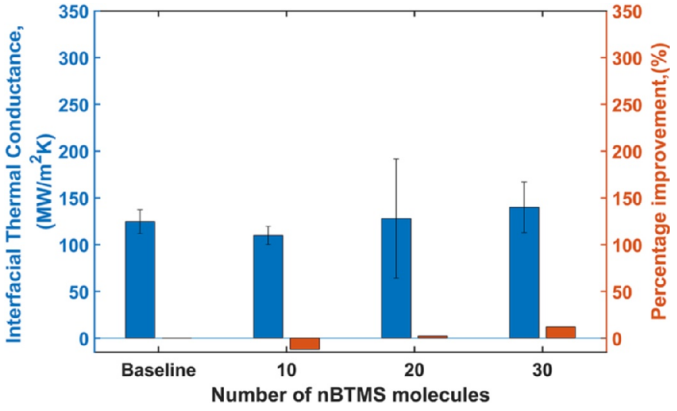


**Fig. 9.** Comparison of computed interfacial thermal conductance for 10, 20 and 30 nBTMS molecules with the baseline case without molecular bridging.

the extent of improvement in interfacial thermal conductance is significantly lower for MPTMS – 10%, 59% and 11% for 10, 20 and 30 molecules, respectively. This shows that the specific end-group being attached to the separator side of the interface plays a key role in determining the effectiveness of molecular bridging, with the amine group in APTES appearing to perform better than the thiol group in MPTMS. Similar to APTES, we also see a non-monotonic behaviour, although for 30 molecule case (rather than 20 molecule case as in APTES).

Simulations are also carried out for molecular bridging with nBTMS that has a methyl end-group, as shown in Fig. 1(c). These results, summarized in Fig. 9, show that there is no significant improvement in interfacial thermal conductance in this case. With 10 molecules of nBTMS, interfacial thermal conductance actually reduces slightly compared to the baseline, whereas the improvement with 20 and 30 molecules is relatively minor.

Figs. 7–9 clearly show the importance of careful selection of bridging molecules for improving interfacial thermal conductance. In general, it can be deduced that good interfacial bonding between the bridging molecule and cathode/separator can result in improved thermal transport compared to the baseline case with only weak van der Waals bonding directly between the cathode and separator. Results indicate better performance of APTES compared to MPTMS and nBTMS. It is also noted in all simulations that thermal conductance does not show a monotonically increase trend in any of the studied cases. The non-monotonicity is observed at different molecular thicknesses (different number of molecules) of each of the case, i.e., 20 silane molecules for APTES, 30 silane molecules for MPTMS, and 10 silane molecules for nBTMS. We hypothesize that these differences in the observation of non-monotonicity could be associated with insufficient molecular relaxations (diffused interface between small molecules and the polymer with varying degree of free volume within the diffused region) in different simulations. If it were to happen due to a physical phenomenon (for example, insufficient silane molecules on the surface) associated with thermal transport, we would have expected the non-monotonicity to occur at certain concentrations (number of molecules) of silanes. The reasoning as pertains to the former hypothesis (insufficient molecular relaxation) is discussed below.

In each of the studies discussed here, equilibration is performed prior to thermal transport simulations for a constant amount of time with the assumption that it will lead to best-possible interface between the molecules and polymer chains. Given the vastness of conformational space of these molecules, as well as long conformational relaxation times of the polymer, realistically, only a tiny fraction of this conformational space can be explored using MD simulations. Here, the equilibration often results in a local minima in vast polymeric conformational space, the spatial configuration of which may have some implications on investigated properties. A visual inspection of the interface region between the molecules and polymer chain did show varying degree of free volume, even after equilibrating for extended periods of time. This varying degree by which polymer chains are relaxing at the interface region may be partly responsible for the observed non-monotonicity.

In order to validate our hypothesis, we perform additional simulations on some of the cases to see if applying external pressure while equilibrium lead to better thermal transport across the region. In this context, simulations for nBTMS are repeated, where we apply an external pressure of 100 atm. during equilibration of additional 5 ns, followed by equilibration to minimize the free volume at the interface, before final equilibration at 1 atm pressure for another 5 ns, prior to thermal transport simulations. After final equilibration, a reduction of around 4 Å in the total length of the simulation box is observed, which suggests better packing of the chains and molecules at the interface region. A case of representative differences in the free volume prior and after the 100 atm. equilibration simulations are visually depicted in Supplementary Information [51] as obtained within the framework of OVITO software [52]. The results are summarized in Fig. 10, showing significant improvement of 128% and 105% improvement with 20 and 30 nBTMS molecules, respectively, with respect to cases when no additional external pressure is applied.

## 4. Conclusions

Thermal transport in Li-ion cell materials is an important phenomenon to study since Li-ion cells overheat very easily, leading to important safety and performance in many practical engineering systems. It is important to identify and address the fundamental root cause of poor thermal conduction within the cell. MD simulations can be an

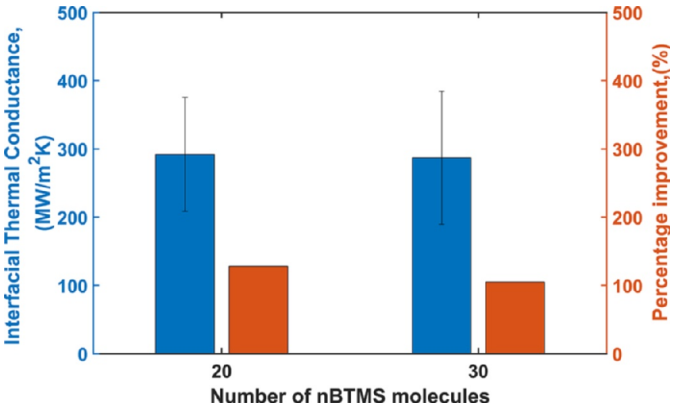


**Fig. 10.** Impact of external pressure on interfacial thermal conductance improvement for nBTMS molecules. Values of interfacial thermal conductance from Fig. (9) (blue) for 20 and 30 nBTMS molecules are used as a baseline to calculate percentage increase.

important tool for such investigation, since simulation results may help identify promising molecules for interfacial bridging that can then be investigated through experiments. Results from this work indicate up to 250% improvement in interfacial thermal conductance with the use of APTES as the bridging molecule. The simulations described in this paper help develop MD simulation capabilities for Li-ion cell related materials, for which validated force-fields were not previously available. Further, the results on the impact of molecular bridging confirm experimental observations reported in the past, thereby helping address an important thermal transport challenge in Li-ion cells.

It must be noted that candidate molecules for interfacial bridging must be compatible with other electrochemical materials inside the Li-ion cell and must not adversely affect cell operation, lifetime and safety. A limited amount of experimental data indicates that molecular bridging with APTES does not adversely affect cell performance [13], but clearly, much more experimental characterization is needed. Further, the long-term stability of molecular bridging with the molecules studied here must be established through measurements. It is expected that MD-based investigations such as the work presented here may help in this direction.

**Supporting Information**

Visualization of free volume within the simulation cell before and after the 100 atm simulations.

## Data Availability Statement

The raw/processed data required to reproduce these findings cannot be shared at this time as the data also forms part of an ongoing study.

## CRediT authorship contribution statement

**Abhijeet Dhakane:** Data curation, Formal analysis, Methodology, Visualization, Writing - original draft, Writing - review & editing. **Vikas Varshney:** Conceptualization, Methodology, Visualization, Writing - original draft, Writing - review & editing. **Juan Liu:** Formal analysis, Methodology, Writing - original draft, Writing - review & editing. **Hendrik Heinz:** Formal analysis, Methodology, Writing - original draft, Writing - review & editing. **Ankur Jain:** Conceptualization, Data curation, Funding acquisition, Project administration, Supervision, Visualization, Writing - original draft, Writing - review & editing.

## Declaration of Competing Interest

The authors declare that they have no known competing financial interests or personal relationships that could have appeared to influence the work reported in this paper.

## Acknowledgments

This material is based upon work supported by CAREER Award No. CBET-1554183 from the National Science Foundation.

## Supplementary materials

Supplementary material associated with this article can be found, in the online version, at doi:10.1016/j.surfin.2020.100674.

## References

[1] D.G. Cahill, W.K. Ford, K.E. Goodson, G.D. Mahan, A. Majumdar, H.J. Maris, R. Merlin, S.R. Phillpot, Nanoscale thermal transport, J. Appl. Phys. 93 (2) (2003) 793–818.
[2] B. Scrosati, J. Garche, Lithium batteries: Status, prospects and future, J. Power Sources 195 (9) (2010) 2419–2430.
[3] G. Karimi, X. Li, Thermal management of lithium-ion batteries for electric vehicles, Int. J. Energy Res. 37 (1) (2013) 13–24.
[4] K. Shah, V. Vishwakarma, A. Jain, Measurement of multiscale thermal transport phenomena in Li-ion cells: A review, J. Electrochem. Energy Convers. Storage 13 (3) (2016) 030801.
[5] T.M. Bandhauer, S. Garimella, T.F. Fuller, A critical review of thermal issues in lithium-ion batteries, J. Electrochem. Soc. 158 (3) (2011) R1–R25.
[6] R. Spotnitz, J. Franklin, Abuse behavior of high-power, lithium-ion cells, J. Power Sources 113 (1) (2003) 81–100.
[7] K. Shah, D. Chalise, A. Jain, Experimental and theoretical analysis of a method to predict thermal runaway in Li-ion cells, J. Power Sources 330 (2016) 167–174.
[8] D. Anthony, D. Wong, D. Wetz, A. Jain, Improved thermal performance of a Li-ion cell through heat pipe insertion, J. Electrochem. Soc. 164 (6) (2017) A961–A967.
[9] L.W. Jin, P.S. Lee, X.X. Kong, Y. Fan, S.K. Chou, Ultra-thin minichannel LCP for EV battery thermal management, Appl. Energy 113 (2014) 1786–1794.
[10] X.M. Xu, R. He., Research on the heat dissipation performance of battery pack based on forced air cooling, J. Power Sources 240 (2013) 33–41.
[11] K. Shah, S.J. Drake, D.A. Wetz, J.K. Ostanek, S.P. Miller, J.M. Heinzel, A. Jain, An experimentally validated transient thermal model for cylindrical Li-ion cells, J. Power Sources 271 (2014) 262–268.
[12] I. Esho, K. Shah, A. Jain, Measurements and modeling to determine the critical temperature for preventing thermal runaway in Li-ion cells, Appl. Therm. Eng. 145 (2018) 287–294.
[13] V. Vishwakarma, C. Waghela, Z. Wei, R. Prasher, S.C. Nagpure, L. Li, F. Liu, C. Daniel, A. Jain, Heat transfer enhancement in a lithium-ion cell through improved material-level thermal transport, J. Power Sources 300 (2015) 123–131.
[14] S.J. Drake, D. Wetz, J. Ostanek, S. Miller, J. Heinzel, A. Jain, Measurement of anisotropic thermophysical properties of cylindrical Li-ion cells, J. Power Sources 252 (2014) 298–304.
[15] J. Zhang, B. Wu, Z. Li, J. Huang, Simultaneous estimation of thermal parameters for large-format laminated lithium-ion batteries, J. Power Sources 259 (2014) 106–116.
[16] D. Chalise, K. Shah, R. Prasher, A. Jain, Conjugate heat transfer analysis of thermal management of a Li-ion battery pack, J. Electrochem. Energy Convers. Storage 15 (1) (2018) 011008.
[17] X. Xu, L. Pereira, Y. Wang, et al., Length-dependent thermal conductivity in suspended single-layer graphene, Nat. Commun. 5 (2014) 3689.
[18] Eric T. Swartz, R.O. Pohl, Thermal boundary resistance, Rev. Mod. Phys. 61 (3) (1989) 605.
[19] P. O'Brien, S. Shenogin, J. Liu, et al., Bonding-induced thermal conductance enhancement at inorganic heterointerfaces using nanomolecular monolayers, Nat. Mater. 12 (2) (2013) 118.
[20] S. Kaur, N. Raravikar, B. Helms, R. Prasher, D. Ogletree, Enhanced thermal transport at covalently functionalized carbon nanotube interfaces, Nat. Commun. 5 (2014) 3082.
[21] X. Wang, J. Zhang, Y. Chen, P. Chan, Investigation of interfacial thermal transport across graphene and an organic semiconductor using molecular dynamics simulations, PCCP 19 (24) (2017) 15933–15941.
[22] T. Feng, Y. Zhong, J. Shi, X. Ruan, Unexpected high inelastic phonon transport across solid-solid interface: Modal nonequilibrium molecular dynamics simulations and Landauer analysis, Phys. Rev. B 99 (4) (2019) 045301.
[23] J. Zhang, Y. Hong, Z. Tong, Z. Xiao, H. Bao, Y. Yue, Molecular dynamics study of interfacial thermal transport between silicene and substrates, PCCP 17 (37) (2015) 23704–23710.
[24] Y.-Y. Zhang, Q.-X. Pei, Y.-W. Mai, S.-K. Siu-Kai Lai, Interfacial thermal conductance in multilayer graphene/phosphorene heterostructure, J. Phys. D Appl. Phys. 49 (46) (2016) 465301.
[25] M. Hu, P. Keblinski, P.K. Schelling, Kapitza conductance of silicon–amorphous polyethylene interfaces by molecular dynamics simulations, Phys. Rev. B 79 (10) (2009) 104305.
[26] L. Hu, L. Zhang, M. Hu, J.-S. Wang, B. Li, P. Keblinski, Phonon interference at self-assembled monolayer interfaces: Molecular dynamics simulations, Phys. Rev. B 81

(23) (2010) 235427.
[27] J. He, L. Zhang, L. Liu, Thermal transport in monocrystalline and polycrystalline lithium cobalt oxide, PCCP (2019), https://doi.org/10.1039/C9CP01585J press.
[28] Hui Y., J.-Y. Yang, C. Savov, et al., Highly Anisotropic Thermal Transport in LiCoO2, J. Phys. Chem. Lett. 10 (18) (2019) 5552–5556.
[29] S. Onclin, B.J. Ravoo, D.N. Reinhoudt, Engineering silicon oxide surfaces using self-assembled monolayers, Angew. Chem. Int. Ed. 44 (39) (2005) 6282–6304.
[30] G. Cappelletti, S. Ardizzone, D. Meroni, et al., Wettability of bare and fluorinated silanes: a combined approach based on surface free energy evaluations and dipole moment calculations, J. Colloid Interface Sci. 389 (1) (2013) 284–291.
[31] D. Meroni, S. Ardizzone, G. Cappelletti, et al., Interplay between chemistry and texture in hydrophobic TiO2 hybrids, J. Phys. Chem. C 115 (38) (2011) 18649–18658.
[32] N. Herzer, C. Haensch, S. Hoeppener, U. Schubert, Orthogonal functionalization of silicon substrates using self-assembled monolayers, Langmuir 26 (11) (2010) 8358–8365.
[33] M.D. Losego, M. Grady, N. Sottos, D. Cahill, P. Braun, Effects of chemical bonding on heat transport across interfaces, Nat. Mater. 11 (6) (2012) 502.
[34] V. Varshney, A.K. Roy, T.J. Michalak, J. Lee, B.L. Farmer, Effect of curing and functionalization on the interface thermal conductance in carbon nanotube–epoxy composites, JOM – J. Minerals Metals Mater. Soc. 65 (2) (2013) 140–146.
[35] H. Heinz, T.-J. Lin, R.K. Mishra, F.S. Emami, Thermodynamically consistent force fields for the assembly of inorganic, organic, and biological nanostructures: the INTERFACE force field, Langmuir 29 (6) (2013) 1754–1765.
[36] H. Heinz, H. Ramezani-Dakhel, Simulations of Inorganic–Bioorganic Interfaces to Discover New Materials: Insights, Comparisons to Experiment, Challenges, and Opportunities, Chem. Soc. Rev. 45 (2016) 412–448.
[37] Pnina Dauber-Osguthorpe, et al., Structure and energetics of ligand binding to proteins: Escherichia coli dihydrofolate reductase-trimethoprim, a drug-receptor system, Proteins Struct. Funct. Bioinf. 4 (1) (1988) 31–47.
[38] Jon R. Maple, et al., Derivation of class II force fields. I. Methodology and quantum force field for the alkyl functional group and alkane molecules, J. Comp. Chem. 15 (2) (1994) 162–182.
[39] H. Heinz, U.W. Suter, Atomic Charges for Classical Simulations of Polar Systems, J. Phys. Chem. B 108 (2004) 18341–18352.
[40] Y. Takahashi, Y. Gotoh, J. Akimoto, S. Mizuta, K. Tokiwa, T. Watanabe, Anisotropic electrical conductivity in LiCoO2 single crystal, J. Solid State Chem. 164 (1) (2002) 1–4.
[41] X. Wang, I. Loa, K. Kunc, K. Syassen, M. Amboage, Effect of pressure on the structural properties and Raman modes of LiCoO2, Phys. Rev. B 72 (22) (2005) 224102.
[42] E.J. Cheng, N.J. Taylor, J. Wolfenstine, J. Sakamoto, Elastic properties of lithium cobalt oxide (LiCoO2), J. Asian Ceramic Soc. 5 (2) (2017) 113–117.
[43] Varshney, V., Patnaik, S.S., Roy, A.K., Farmer, B.L., “A molecular dynamics study of epoxy-based networks: cross-linking procedure and prediction of molecular and material properties.” Macromolecules41 (18), 6837-6842.
[44] Varshney, V., Patnaik, S.S., Roy, A.K., Farmer, B.L., “Modeling of Thermal Conductance at Transverse CNT − CNT Interfaces.” J. Phys. Chem. C114 (39), 16223-16228.
[45] S. Plimpton, Fast parallel algorithms for short-range molecular dynamics, J. Comput. Phys. 117 (1) (1995) 1–19.
[46] BIOVIA, Dassault Systèmes. "Discovery studio visualizer, Release 2017, San Diego: Dassault Systèmes, 2016." Available athttp://accelrys.com/products/collaborative-science/biovia-discovery-studio/visualization-download. *php* (accessed Oct 27, 2019).
[47] R.W. Hockney, J.W. Eastwood, Computer Simulation Using Particles, Adam Hilger, NY, 1989.
[48] Anderson, C., Tamma, K., ‘An overview of advances in heat conduction models and approaches for prediction of thermal conductivity in thin dielectric films,’ Int. J. Numer. Methods Heat Fluid Flow14(1), 12-65.
[49] Varshney, V., Roy, A.K., Baur, J.W., ‘Modeling the Role of Bulk and Surface Characteristics of Carbon Fiber on Thermal Conductance across the Carbon-Fiber/Matrix Interface.’ ACS Appl. Mater. Interfaces7 (48), 26674-26683.
[50] V. Vishwakarma, A. Jain, Measurement of in-plane thermal conductivity and heat capacity of separator in Li-ion cells using a transient DC heating method, J. Power Sources 272 (2014) 378–385.
[51] Supplementary Information for this paper is available at doi.org/…doi:10.1016/j.surfin.2020.100674.
[52] A. Stukowski, Visualization and analysis of atomistic simulation data with OVITO–the Open Visualization Tool, Model. Simul. Mater. Sci. Eng. 18 (2009) 015012.